DOI: 10.1002/ejic.200801086

Pyrazole and Pyrazolyl Complexes of *cis*-Bis(2,2′-bipyridine)-chlororuthenium(II): Synthesis, Structural and Electronic Characterization, and Acid-Base Chemistry

Hershel Jude,[a] Francisca N. Rein,[b] Weizhong Chen,[a] Brian L. Scott,[c] Dana M. Dattelbaum,*[d] and Reginaldo C. Rocha*[a]

Keywords: Ruthenium / Pyrazole / Pyrazolate / Acidity / Hydrogen bonds

Complexes of the type *cis*-$[Ru(bpy)_2(Cl)(L)]^+$ [bpy = 2,2′-bipyridine; with L = pyrazole (**1H**), 4-methylpyrazole (**2H**), and 3,5-dimethylpyrazole (**3H**)] were synthesized and isolated as hexafluorophosphate salts. The molecular structures of these new complexes were fully characterized by ^{1}H NMR spectroscopy and ESI mass spectrometry, and the crystal structure of **3H**·PF_6 was determined by X-ray crystallography. Compound **3H**·PF_6 ($C_{25}H_{24}ClF_6N_6PRu$) crystallizes in the monoclinic space group $P2_1/n$ with a = 12.102(2) Å, b = 16.826(3) Å, c = 13.016(2) Å, β = 92.606(2)°, V = 2647.6(8) Å^3, and Z = 4. The crystal structure of **3H** reveals the formation of an intramolecular hydrogen bond (2.562 Å) between the pyrazole N(2)–H site and the chloride ligand. The redox and electronic absorption properties of **1H**, **2H**, and **3H**, as well as their deprotonated counterparts [L = pyrazolate (**1**), 4-methylpyrazolate (**2**), and 3,5-dimethylpyrazolate (**3**)], were investigated by cyclic voltammetry and UV/Vis spectroscopy. For detailed analysis of the electronic nature of this series of pyrazolyl ligands, the results are discussed along with other relevant *cis*-$[Ru(bpy)_2(X)(Y)]^{n+}$ complexes. From spectrophotometric pH titrations, the basicity associated with the coordinated pyrazole/pyrazolate couple in water was found in all three cases to be unusually high, partly owing to the N–H···Cl hydrogen bond that stabilizes the protonated, azole state.

Introduction

Polypyridyl complexes of ruthenium(II) of the type *cis*-$[Ru(bpy)_2(X)(Y)]^{n+}$ have played a very important role in inorganic chemistry owing to their versatile synthetic chemistry, rich redox chemistry, and electrochemical and photophysical/photochemical properties of relevance to several application areas such as electrocatalysis and photocatalysis.[1] However, while complexes with a variety of N-heterocyclic X/Y ligands abound, examples containing five-membered ring ligands with weak π-acceptor or π-donor properties such as pyrazoles or pyrazolates have received less attention, despite the vastly explored and established coordination chemistry of complexes with bis-, tris-, or poly-pyrazolyl derivatives such as tris(pyrazolyl)borates and tris(pyrazolyl)alkanes.[2]

Although a few (multi)bridged dimeric complexes of $Ru(bpy)_2$ with a pyrazolyl or substituted pyrazolyl-bridging group are known,[3–5] only one bis-pyrazole $Ru(bpy)_2$ complex has been studied,[3] and no mono-pyrazole/pyrazolyl example was known to date. The same applies to other imidazoles[5–7] and triazoles,[5,7,8] although several examples of mono-azole/azolyl complexes exist for these ligands. Owing to their capability for (de)protonation at the ionizable NH site, azoles are also interesting as ligands because they can reversibly switch from weak π-acceptors in the protonated form (azole) to π-excessive, strong donors in the deprotonated form (azolate).[5]

Here we report the synthesis, structural characterization, and electrochemical and spectroscopic studies of the complexes *cis*-$[Ru(bpy)_2(Cl)(L)]^{n+}$ (bpy = 2,2′-bipyridine) with L = pyrazole (pzH), 4-methylpyrazole (MepzH), and 3,5-dimethylpyrazole (Me_2pzH) and their corresponding deprotonated pyrazolate forms (with L = pz$^-$, Mepz$^-$, and Me_2pz$^-$ anions). Spectrophotometric measurements as a function of pH were systematically performed as an attempt to determine the acid dissociation contants (K_a) with respect to the pyrazole/pyrazolate ionization process in aqueous solutions (Scheme 1).

[a] Materials Physics and Applications Division, Center for Integrated Nanotechnologies, MPA-CINT, Los Alamos National Laboratory,
Los Alamos, New Mexico, NM 87545, USA
E-mail: rcrocha@lanl.gov
[b] Chemistry Division, Physical Chemistry and Applied Spectroscopy, C-PCS, Los Alamos National Laboratory,
Los Alamos, New Mexico, NM 87545, USA
[c] Materials Physics and Applications Division, Materials Chemistry, MPA-MC, Los Alamos National Laboratory,
Los Alamos, New Mexico, NM 87545, USA
[d] Dynamic and Energetic Materials Division, Shock and Detonation Physics, DE-9, Los Alamos National Laboratory,
Los Alamos, New Mexico, NM 87545, USA
E-mail: danadat@lanl.gov
Supporting information for this article is available on the WWW under http://www.eurjic.org or from the author.

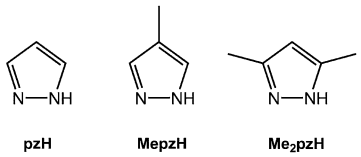

Scheme 1.

Results and Discussion

Synthesis and Characterization

Complexes $[Ru(bpy)_2(Cl)(pzH)]^+$ (**1H**), $[Ru(bpy)_2(Cl)(MepzH)]^+$ (**2H**), and $[Ru(bpy)_2(Cl)(Me_2pzH)]^+$ (**3H**) were prepared in good yields (> 75%) by refluxing *cis*-$Ru(bpy)_2Cl_2$ hydrate in methanol with 1 equiv. of the appropriate pyrazole ligand for 8 h. Samples of these complexes were isolated as PF_6^- salts in pure form, without the need for further purification. These compounds are very soluble in polar solvents such as acetonitrile, dichloromethane, acetone, and dimethylformamide.

NMR Spectra

The ^1H NMR spectra of **1H**–**3H** in CD_2Cl_2 and CD_3CN are available as Supporting Information (Figures S1–S12). For simplicity, the following discussion concerns only the spectra recorded in CD_2Cl_2. No resonances are present between 1–6 ppm in the ^1H NMR spectrum of **1H**. However, in the spectra of **2H** and **3H** there are one (δ = 1.92 ppm) and two (1.19 and 2.23 ppm) singlet resonances, respectively, corresponding to the methyl protons of the 4-MepzH and 3,5-Me_2pzH ligands. In the spectrum of free, uncoordinated 4-MepzH and 3,5-Me_2pzH, a single singlet resonance is observed at δ = 2.10 and 2.25 ppm, respectively, in CD_2Cl_2. The resonances due to the methyl protons are slightly shifted downfield in the spectra of the corresponding complexes with respect to the free ligands. Further evidence for $Ru–N_{pyrazole}$ coordination in **3H** comes from the presence of two well-separated resonances in the spectrum of the complex (1.19 and 2.23 ppm) compared to a single one in the free ligand (δ = 2.25 ppm), owing to the difference in geometric distances from the metal center to each of the methyl groups in 3,5-Me_2pzH (see Figure 2 below). Between 5.7 and 6.5 ppm are the resonances arising from the pyrazole ring CH protons. The resonances at δ = 6.30 and 6.40 ppm for **1H**, 6.17 ppm for **2H**, and 5.77 ppm for **3H** are shifted downfield of those observed for the free ligands (pzH: 7.66 and 6.36 ppm; 4-MepzH: 7.39 ppm; 3,5-Me_2pzH: 5.82 ppm). The aromatic region between δ = 7 and 9 ppm is surprisingly free of very many overlapping peaks, considering that 16 different resonances corresponding to the bpy CH protons are predicted due to the low symmetry in these complexes. These peaks integrate to give the expected number of protons (16 H) for all three complexes. A broad resonance is observed above 12 ppm (**1H**, 12.61; **2H**, 12.33; and **3H**, 12.20 ppm), and is attributed to the pyrazole NH protons. The downfield shift shown by the comparison of the chemical shifts for the NH proton in the free, uncoordinated pyrazole (δ = 11.90 ppm) with that in the corresponding complex **1H** (δ = 12.61 ppm) is consistent with the intramolecular N–H···Cl interaction that was clearly manifested in the X-ray crystal structure discussed below.

Mass Spectra

The monocations **1H**, **2H**, and **3H** were also structurally characterized by ESI-MS. The isotopically resolved 1+ charge states for complexes **1H**–**3H** are shown in Figure 1. These charge states are in excellent agreement with the predicted isotopic distribution patterns. The full mass spectra with assignments noted for **1H**–**3H** are available as Supporting Information (Figures S13–S18). A series of four peaks are observed in the mass spectra of all three complexes. For **1H**, these peaks are observed at *m*/*z* = 516.99, 480.99, 448.91, and 412.95, corresponding to the charge states $[Ru(bpy)_2(Cl)(pzH)]^+$, $\{Ru(bpy)_2(pzH)\}^+$, $\{Ru(bpy)_2(Cl)\}^+$, and $\{Ru(bpy)_2\}^+$, respectively. The analogous set of four peaks is observed at *m*/*z* = 531.00, 495.06, 448.92, and 412.99 for **2H**, and at *m*/*z* = 545.03, 509.01, 448.88, and 412.99 for **3H**.

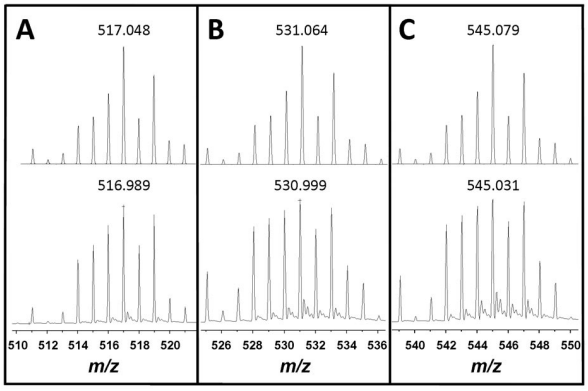

Figure 1. Electrospray ionization quadrupole mass spectra of (A) **1H**, (B) **2H**, and (C) **3H**. The calculated and experimental isotopic distribution patterns are shown at the top and bottom, respectively.

Crystal Structure

The molecular structure of **3H**·PF_6 was confirmed by single-crystal X-ray diffraction. Crystals were grown by vapor diffusion of diethyl ether into acetonitrile solutions of the complex. Thermal ellipsoid diagrams of the cation is shown in Figure 2 and selected bond lengths and angles are summarized in Table 1. The geometry about the Ru center is a distorted octahedral, with angles from 79 to 98° and from 173 to 177°, which are consistent with those typically observed for polypyridyl Ru^{II} complexes.[4,9] The pyridyl and pyrazole rings are planar and the bpy ligands adopt a *cis* configuration. The longer $Ru–N_{pzH}$ distance relative to the $Ru–N_{bpy}$ distances is a consequence of the weaker π-acceptor character of the pyrazole ligand compared to bpy

pyridyl groups. As expected, the bpy N(6) atom *trans* to the strongly donor Cl^- ligand exhibits the shortest Ru–N bond length, owing to the increased $Ru^{II} \rightarrow N_{bpy}$ π-backbonding interaction.

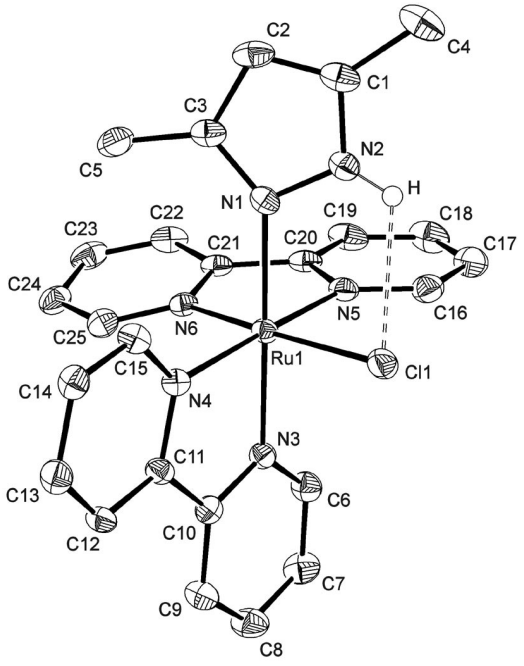

Figure 2. Single-crystal X-ray structure of **3H**·PF_6. Except for H(2), all H atoms and the PF_6^- counterion are omitted for clarity (thermal ellipsoid plot drawn at 50% probability).

Table 1. Selected bond lengths [Å] and angles [°] for **3H**·PF_6.

Distances [Å]		Angles [°]	
Ru(1)–N(1)	2.109(3)	N(3)–Ru(1)–N(1)	176.67(11)
Ru(1)–N(3)	2.042(3)	N(4)–Ru(1)–N(1)	97.65(11)
Ru(1)–N(4)	2.054(3)	N(5)–Ru(1)–N(1)	86.00(11)
Ru(1)–N(5)	2.048(3)	N(6)–Ru(1)–N(1)	92.57(11)
Ru(1)–N(6)	2.016(3)	N(3)–Ru(1)–N(4)	79.32(11)
Ru(1)–Cl(1)	2.4078(9)	N(5)–Ru(1)–N(4)	175.62(11)
N(1)–N(2)	1.357(4)	N(6)–Ru(1)–N(4)	98.28(11)
N(2)–C(1)	1.350(4)	N(3)–Ru(1)–N(5)	97.08(12)
C(1)–C(4)	1.487(5)	N(6)–Ru(1)–N(3)	89.25(11)
C(1)–C(2)	1.355(5)	N(6)–Ru(1)–N(5)	79.07(12)
C(2)–C(3)	1.414(5)	N(1)–Ru(1)–Cl(1)	88.42(8)
C(3)–C(5)	1.489(5)	N(3)–Ru(1)–Cl(1)	90.07(9)
C(3)–N(1)	1.335(4)	N(4)–Ru(1)–Cl(1)	87.84(8)
N(3)–C(6)	1.339(4)	N(5)–Ru(1)–Cl(1)	94.70(9)
C(6)–C(7)	1.378(5)	N(6)–Ru(1)–Cl(1)	173.60(8)
C(7)–C(8)	1.372(5)	Ru(1)–N(1)–N(2)	116.2(2)
C(8)–C(9)	1.374(5)	N(1)–N(2)–C(1)	112.1(3)
C(9)–C(10)	1.385(5)	N(2)–C(1)–C(2)	105.9(3)
C(10)–N(3)	1.359(4)	C(1)–C(2)–C(3)	107.4(3)
C(10)–C(11)	1.460(4)	C(2)–C(3)–N(1)	108.6(3)
N(2)–Cl(1)	3.063	N(3)–C(6)–C(7)	123.2(3)
N(2)–H	0.859	C(7)–C(8)–C(9)	119.3(4)
N(2)–H···Cl(1)	2.562	C(9)–C(10)–C(11)	123.7(3)
		N(2)–H···Cl	118.2

Particularly relevant to the acid-base properties of **1H/1**, **2H/2**, and **3H/3** (discussed below) is the fact that the crystal structure of **3H** reveals the formation of an intramolecular hydrogen bond between the pyrazole N(2)–H site and the equatorially coordinated Cl^- ligand (Table 1; shown in Figure 2). The H···Cl distance of 2.562 Å is significantly shorter than the sum of the van der Waals radii for hydrogen and chlorine (2.95 Å). NMR and IR spectra[10] for acetonitrile solutions provide evidence for the presence of strong N–H···Cl interactions in liquid phase as well.

Although crystallographic structural data are not uncommon for complexes with deprotonated pyrazolates (pz) and derivatives such as tris(pyrazolyl)borate and tris(pyrazolyl)methane ligands, X-ray crystal structures of only a few Ru^{II} complexes with a protonated pyrazole group (pzH) are available[11,12] and no example involving polypyridines has been previously reported. In general, the Ru–N_{pzH} distance of 2.113(3) Å observed for **3H**·PF_6 is similar to those found in the literature. Interestingly, however, in some cases the protonation states of the ligand (i.e. pzH vs. pz) do not appear to affect much the Ru–N bond lengths.[11]

The Ru–N_{bpy} distances in the single crystals of **3**·PF_6 are 2.019(3), 2.041(3), 2.049(3), and 2.054(3) Å, and are in the range of typical values for *cis*-$Ru^{II}(bpy)_2$ complexes. For example, the Ru–N_{bpy} distances in crystals of $Ru(bpy)_2Cl_2$ are 2.013–2.054 Å, with the shortest Ru–N bonds *trans* to the Ru–Cl ones.[9] The Ru–Cl bond length of 2.4078(9) Å in **3H**·PF_6 is also comparable to those for $Ru(bpy)_2Cl_2$ (2.426 Å),[9] and $[Ru(tpm)(bpy)(Cl)]PF_6$ [2.411 Å; tpm = tris(pyrazolyl)methane].[13]

Electronic Properties

Electrochemistry

The cyclic voltammograms of **1H**, **2H**, and **3H** in acetonitrile exhibit reversible Ru^{II}/Ru^{III} oxidations at 0.81, 0.79, and 0.79 V (vs. SCE), respectively (Table 2). Upon replacing one of the Cl^- ligands of the starting material $Ru(bpy)_2Cl_2$ (0.32 V (vs. SCE) in acetonitrile/0.1 M NEt_4ClO_4)[14] with the pyrazole ligand, the metal center becomes more difficult to oxidize by nearly 0.5 V. This positive shift in the potential was also observed for the related complex with pyridine, $[Ru(bpy)_2(Cl)(py)]^+$ (0.79 V (vs. SCE) in acetonitrile/0.1 M NEt_4ClO_4),[14] and is due to substitution of the anionic, electron donating Cl^- with the neutral, π-accepting ligand. When both Cl^- ligands are substituted with pzH or py, the oxidation potentials of the complexes, $[Ru(bpy)_2(pzH)_2]^{2+}$ (1.18 V (vs. SCE) in acetonitrile/0.1 M Bu_4NPF_6)[3] and $[Ru(bpy)_2(py)_2]^{2+}$ (1.30 V (vs. SCE) in acetonitrile/0.1 M NEt_4ClO_4),[14] are further upshifted by about 0.4 and 0.5 V relative to the $[Ru(bpy)_2(Cl)(L)]^+$ counterparts. Both comparisons confirm that pyrazole and pyridine have comparable electronic character as weak π-acceptors, as also noted earlier.[3]

Upon ligand deprotonation of **1H**, **2H**, and **3H** in dry acetonitrile using Me_4NOH (see experimental details), the Ru^{II}/Ru^{III} processes for **1**, **2**, and **3** appeared at 0.28, 0.25, and 0.20 V (vs. SCE), respectively (Table 2). This downshift of >0.5 V reflects the added negative charge and the transition of electronic character of the ligand from weak π-acceptor in the protonated pyrazole form (which is compar-

Table 2. Summary of redox potentials and UV/Vis absorption spectral properties for the pyrazole complexes **1H**, **2H**, and **3H**, and their deprotonated pyrazolate counterparts **1**, **2**, and **3** in acetonitrile. Other relevant complexes are also included for comparison.[a]

Complex	Redox potential $E_{1/2}$ (Ru^{II}/Ru^{III})/V (vs. SCE)	Absorption data ε_{max} [nm] (λ [$M^{-1}cm^{-1}$])
$[Ru(bpy)_2(Cl)(pzH)]^+$ (**1H**)	0.81	500 (9.0×10^3) 350 (7.9×10^3) 290 (3.6×10^4) 246 (2.0×10^4)
$[Ru(bpy)_2(Cl)(MepzH)]^+$ (**2H**)	0.79	504 (8.8×10^3) 352 (7.8×10^3) 288 (4.0×10^4) 246 (2.0×10^4)
$[Ru(bpy)_2(Cl)(Me_2pzH)]^+$ (**3H**)	0.79	504 (9.1×10^3) 352 (8.2×10^3) 288 (4.3×10^4) 246 (2.2×10^4)
$Ru(bpy)_2(Cl)(pz)$ (**1**)	0.28	560 (7.9×10^3) 380 (9.0×10^3) 294 (3.4×10^4) 242 (2.5×10^4)
$Ru(bpy)_2(Cl)(Mepz)$ (**2**)	0.25	564 (1.1×10^4) 380 (1.3×10^4) 294 (4.9×10^4) 242 (2.5×10^4)
$Ru(bpy)_2(Cl)(Me_2pz)$ (**3**)	0.20	570 (1.0×10^4) 380 (1.2×10^4) 296 (5.0×10^4) 242 (2.4×10^4)
$Ru(bpy)_2Cl_2$ [b,c]	0.32	553 (9.1×10^3) 380 (8.9×10^3) 297 (5.0×10^4) 243 (2.1×10^4)
$[Ru(bpy)_2(Cl)(py)]^+$ [b,c]	0.79	496 (8.1×10^3) 350 (1.0×10^4) 293 (4.2×10^4) 242 (1.8×10^4)
$[Ru(bpy)_2(py)_2]^{2+}$ [b,c]	1.30	455 (8.2×10^3) 338 (1.6×10^4) 289 (5.0×10^4) 243 (2.4×10^4)
$[Ru(bpy)_2(pzH)_2]^{2+}$ [c]	1.18	470 (5.2×10^3) ca. 323 (ca. 5×10^3) 289 (4.6×10^4) 243 (1.9×10^4)
$[Ru(bpy)_2(pzH)(pz)]^+$ [c]	0.69	510 (4.9×10^3) 363 (4.5×10^3) 292 (4.0×10^4) 250 (ca. 1.5×10^4)
$Ru(bpy)_2(pz)_2\cdot H_2O$[c,d]	0.30	581 (4.6×10^3) 434 (4.1×10^3)

[a] Unless otherwise noted, the electrochemical and spectroscopic data were obtained for acetonitrile solutions; $E_{1/2}$ values are referenced vs. SCE. [b] Ref.[14]. [c] Ref.[3]. [d] DMF solution.

able to pyridine; Table 2) to strongly π-donor in the deprotonated pyrazolate form. Similar shifts were reported for the disubstituted $[Ru(bpy)_2(pzH)_2]^{2+}$ analogue, for which two stepwise deprotonations to give $[Ru(bpy)_2(pzH)(pz)]^+$ and $Ru(bpy)_2(pz)_2$ cause the metal oxidation potential to shift from 1.18 V to 0.69 V and 0.30 V (vs. SCE), respectively.[3] Electrochemical and spectroscopic data for these complexes are also included in Table 2 for comparison.

The fact that the potentials for **2** and **3** are increasingly more negative than that of **1** is consistent with the enhanced electron donation from the addition of methyl substituents into the azole ligand. However, this effect is much less pronounced across the protonated species (for which the $E_{1/2}$ values are very close for **2H** and **3H**), indicating that in the cations the electronic contribution from two methyl groups at ring positions 3,5 is not significantly increased at the coordinating N atom compared to the same effect from a single methyl substituent at position 4 of the pyrazole ring.

UV/Vis Spectra

The UV/Vis absorption spectra of **1H** (Figure 3), **2H**, and **3H** are similar and show two sets of visible absorption bands in the ranges of 400–600 nm (A_{max} at ca. 500 nm) and 300–400 nm (A_{max} at ca. 350 nm), in addition to the strong UV absorptions (A_{max} around 290, 245, and 210 nm). As shown in Table 2, the same spectral pattern has been observed and previously assigned for other comparatively relevant complexes. The visible absorption bands in the two main regions around 400–600 nm (I) and 300–400 nm (II) typically consist of overlapping components that are characteristic of metal-to-ligand charge-transfer (MLCT) processes involving closely spaced transitions from the d_π orbitals of Ru^{II} to the lowest-lying π* orbitals of bpy, i.e. π_1* (region I) and π_2* (region II). The pair of higher-energy UV bands arise from the bpy ligand-centered π→π* transitions to the same set of accessible π* orbitals involved in the MLCT transitions (i.e. π_1* and π_2*).

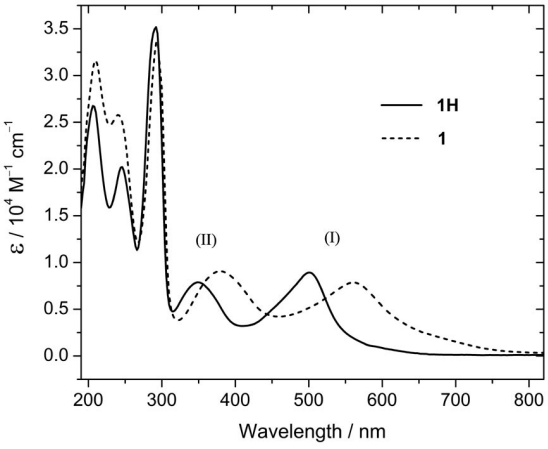

Figure 3. UV/Vis spectra of **1H** (solid line) and **1** (dashed line) in dry acetonitrile.

A dramatic change in the visible absorption spectra of the complexes results from the deprotonation of the bound pyrazole ligands, although the same pattern of two well-defined MLCT absorptions remains. As shown in Figure 3 for **1**, the MLCT(I) and MLCT(II) bands are red-shifted by 60 nm and 30 nm, respectively, relative to **1H** (see also Table 2 for comparison with the spectroscopic data of **2** and **3**). Although these MLCT absorptions involve only pyridyl ligands [i.e. Ru(dπ)→bpy(π*) transitions], the red shifts

originate at electronic effects induced by the transition of the pyrazolyl ligands from weak acceptors in the protonated (azole) form to relatively strong donors in the deprotonated (azolate) form. Ligand deprotonation results in increased charge density on the metal and therefore decreased energy separation between the Ru(dπ) HOMO and the bpy(π*) LUMO levels. For comparison, the redox potentials and MLCT energies of **1H**, **2H**, and **3H** are all very similar to those of $[Ru(bpy)_2(Cl)(py)]^+$ (see Table 2), indicating that the electronic nature of the protonated pyrazoles is comparable to that of pyridine, a known weak π-acceptor ligand. On the other hand, the redox potentials and MLCT energies of **1**, **2**, and **3** are even lower than those of $Ru(bpy)_2Cl_2$ (Table 2), indicating that the deprotonated, anionic pyrazolates are stronger π-donors than the known Cl^- ion as a ligand.

Consistent with the trend in redox potentials, the energies of the MLCT(I) transitions for **1H**, **2H**, **3H** (and **1**, **2**, **3**) follow the order **3H** < **2H** < **1H** (and **3** < **2** < **1**). The lower energies for the complexes of substituted ligands are due to the increasingly greater electron-donating power of the methyl- and dimethyl-pyrazolyl derivatives compared to unsubstituted pyrazolate. Also consistent with the electrochemical results is the observation that the MLCT(I) red shifts accompanying ligand deprotonation are increasingly more pronounced from **1** to **2** to **3** relative to their corresponding protonated species, indicating again that in the deprotonated form these complexes are more sensitive to the mono- and di-substitution of the pyrazole ligand with methyl groups. The observations above are also in agreement with the relative basicities of these ligands (pK_a values are 14.2, 14.9, and 15.1 for pzH, MepzH, and Me_2pzH, respectively).[15] The ligand substitution has negligible effect on the bpy π→π* transitions, for which the absorption energies are essentially identical for **1H**, **2H**, and **3H** (as well as **1**, **2**, and **3**).

Acid-Base Chemistry in Water

As an attempt to spectrophotometrically determine the acid dissociation contants (K_a) with respect to the pyrazole/pyrazolate ionization process in aqueous solutions, the UV/Vis absorption spectra of all complexes were measured as a function of pH (in the pH range from 2 to 14). As shown in Figure 4 for **1H**, the two expected sets of visible absorptions (see above) initially appear with A_{max} at approximately 480 and 330 nm for solutions at pH < 10. As the pH is increased above 10, the absorption maxima of MLCT(I) and MLCT(II) bands progressively shift toward the red region. Following the same rationale discussed above for the acetonitrile solutions, this bathochromic shift with increasing pH is consistent with the conversion of the pyrazole complex into its deprotonated pyrazolate form. A similar behavior was observed for the **2H** and **3H** analogues in water. In all cases, however, the spectra of the samples at the highest obtained pH clearly indicate that the solutions are mixtures of the pyrazole and pyrazolate species in equilibrium. In fact, the deprotonation process does not reach completeness even in solutions at pH 13–14, and the multiwavelength plots of A_{330}/A_{480} vs. pH (Figure 4; inset) show only the upper portion of the typical sigmoidal titration curve, from which the pK_a values cannot be accurately estimated.

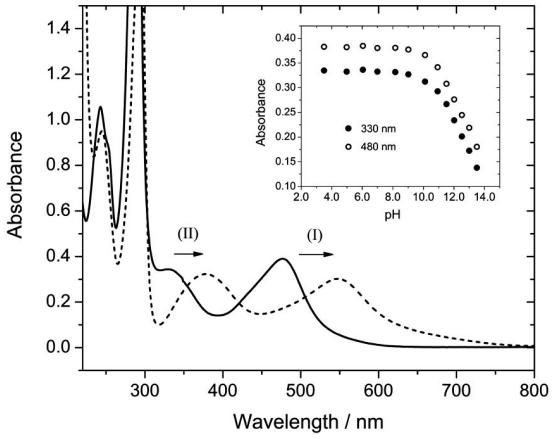

Figure 4. UV/Vis spectra of a 5.5×10^{-5} M solution of **1H** in water (BR buffer) at pH 6 (solid line) and 13 (dashed line). Shown in the inset is the pH dependence of the absorption at two wavelengths (330 and 480 nm) in the pH region 3.5–13.5.

The observed acid-base behavior clearly demonstrates that the pyrazolyl complexes are strong bases, which explain why in the experiments involving the deprotonated species in dry acetonitrile (above) the ligand protonation regenerating the initial pyrazole complexes occurs if any trace of water is present. Given the high pK_a values (> 14)[15] of the uncoordinated ligands, such a basicity for the coordinated ligands is not totally unexpected. However, a significant increase in acidity (decrease in pK_a) is generally observed for the ligand upon metal binding in this type of complexes, owing to their ability to stabilize the azolyl group due to redistribution of charge density via π-donation from the ligand to the Ru center and, effectively, to the π-accepting bpy ligands. Therefore, the enhanced basic character in **1H/1**, **2H/2**, and **3H/3** is presumably caused by the N–H···Cl hydrogen bond (shown in Figure 2 and schematically illustrated below) that promotes the stabilization of the protonated, azole state. A hydrogen bond of the type N–H···N (i.e. pz-H···pz) was also proposed to account for the high basicity of *cis*-$[Ru(bpy)_2(pzH)(pz)]^+$.[3] While the pK_a of this mixed pyrazole/pyrazolate complex was estimated to be > 13, the bis-pyrazole species (*cis*-$[Ru(bpy)_2(pzH)_2]^{2+}$) can be deprotonated even with weak pyridine bases such as collidine.[3] This example provides another illustration of the importance of intramolecular hydrogen bonds between ligands in defining the overall chemical properties of such complexes with azole derivatives (Scheme 2).

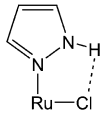

Scheme 2.

Conclusions

The synthesis and structural, electronic and redox characterization of a series of pyrazolyl complexes of *cis*-{$Ru(bpy)_2(Cl)$} are reported. From comparative analysis of these complexes along with other structurally relevant species, it is shown that the electronic nature of the ligands in the protonated (neutral) and deprotonated (anionic) forms is comparable to that of pyridine and chloride ions, respectively. These results confirm previous studies indicating that azoles usually act as weak π-acceptors whereas azolates are strong π-donors as ligands in this type of systems. As assessed from spectrophotometric pH titrations, the basicity associated with the coordinated pyrazole/pyrazolate couple in water was found be unusually high in **1H/1**, **2H/2**, and **3H/3**. This acid-base behavior can, at least in part, be attributed to the stabilization of the protonated, azole state by the intramolecular N–H···Cl hydrogen bond that was revealed by the crystal structure of **3H**. The presence of N–H···Cl interactions in solution phase was also evidenced through NMR and IR spectroscopy.

Experimental Section

Materials: *cis*-$[Ru(bpy)_2Cl_2]$ was prepared as described previously.[16] Pyrazole (pzH; Acros), 4-methylpyrazole (4-MepzH; Acros), 3,5-dimethylpyrazole (3,5-Me_2pzH; Acros), and ammonium hexafluorophosphate (Acros) were used as received. All other reagents and organic solvents were high-purity grade and used without further purification. Acetonitrile used in the preparation of solutions for electrochemical or spectroscopic experiments was anhydrous and stored over 4-Å molecular sieves. Tetrabutylammonium hexafluorophosphate (Bu_4NPF_6; Aldrich) was dried in vacuo prior to its use as supporting electrolyte in solutions for electrochemical experiments. Deionized water from a Nanopure purification system was used in the preparation of aqueous solutions. Sodium trifluoroacetate (NaTFA; Alfa) was employed as supporting electrolyte in the electrochemical measurements in water. 0.1 M Britton-Robinson (BR) buffer[17] and 3.0 M sodium hydroxide (Fisher) and trifluoroacetic acid (HTFA; Fisher) solutions were employed in the pH-controlled experiments (pH 2–12).

Syntheses and Sample Preparations

$[Ru(bpy)_2(Cl)(pzH)](PF_6)$ (1H·PF_6): $Ru(bpy)_2Cl_2·2H_2O$ (1.04 g, 2.0 mmol) and pzH (137 mg, 2.0 mmol) were added to methanol (100 mL). The solution was heated at reflux under Ar (g) for 8 h and cooled to room temperature. The mixture was filtered and 2 mL of a saturated solution of NH_4PF_6 (aq.) was added to the red filtrate. The solution was poured into 800 mL of diethyl ether and the resultant precipitate was collected by vacuum filtration. The red solid was washed with diethyl ether (3 × 20 mL) and dried under vacuum; yield 1.05 g (79%). $C_{23}H_{20}ClF_6N_6PRu$ (661.94): calcd. C 41.73, H 3.05, N 12.70; found C 41.65, H 2.96, N 12.45. ^1H NMR (CD_2Cl_2): δ = 6.30 (m, 1 H, CH_{pzH}), 6.40 (m, 1 H, CH_{pzH}), 7.15 (dd, 1 H, CH), 7.22 (dd, 1 H, CH), 7.51 (d, 1 H, CH), 7.62 (m, 2 H, CH), 7.68 (m, 1 H, CH_{pzH}), 7.78 (m, 2 H, CH), 7.84 (dd, 1 H, CH), 8.01 (m, 2 H, CH), 8.08 (d, 1 H, CH), 8.21 (d, 1 H, CH), 8.24 (d, 1 H, CH), 8.30 (d, 1 H, CH), 8.33 (d, 1 H, CH), 9.94 (d, 1 H, CH), 12.61 (s, 1 H, NH) ppm; see Figures S1–S2. ESI-MS (positive ion mode): *m*/*z* = 516.99 $[Ru(bpy)_2(Cl)(pzH)]^+$, 480.99 $[Ru(bpy)_2(pzH)]^+$, 448.91 $[Ru(bpy)_2(Cl)]^+$, 412.95 $[Ru(bpy)_2]^+$; see Figures S13–S14.

$[Ru(bpy)_2(Cl)(4\text{-}MepzH)](PF_6)$ (2H·PF_6): $Ru(bpy)_2Cl_2·2H_2O$ (1.04 g, 2.0 mmol) and 4-MepzH (186 μL, 2.0 mmol) were added to methanol (100 mL). The solution was heated at reflux under Ar (g) for 8 h and cooled to room temperature. The mixture was filtered and 2 mL of a saturated solution of NH_4PF_6 (aq.) was added to the red filtrate. The solution was poured into 800 mL of diethyl ether and the resultant precipitate was collected by vacuum filtration. The red solid was washed with diethyl ether (3 × 20 mL) and dried under vacuum; yield 1.04 g (77%). ^1H NMR (CD_2Cl_2): δ = 1.92 (s, 3 H, CH_3), 6.17 (s, 1 H, CH_{MepzH}), 7.14 (dd, 1 H, CH), 7.21 (dd, 1 H, CH), 7.44 (s, 1 H, CH_{MepzH}), 7.51 (dd, 1 H, CH), 7.62 (m, 2 H, CH), 7.77 (m, 2 H, CH), 7.84 (dd, 1 H, CH), 8.01 (m, 2 H, CH), 8.09 (d, 1 H, CH), 8.20 (d, 1 H, CH), 8.25 (d, 1 H, CH), 8.31 (m, 2 H, CH), 9.93 (d, 1 H, CH), 12.33 (s, 1 H, NH) ppm; see Figures S5–S6. ESI-MS (positive ion mode): *m*/*z* = 531.00 $[Ru(bpy)_2(Cl)(4\text{-}MepzH)]^+$, 495.06 $[Ru(bpy)_2(4\text{-}MepzH)]^+$, 448.92 $[Ru(bpy)_2(Cl)]^+$, 412.99 $[Ru(bpy)_2]^+$; see Figures S15–S16.

$[Ru(bpy)_2(Cl)(3,5\text{-}Me_2pzH)](PF_6)$ (3H·PF_6): $Ru(bpy)_2Cl_2·H_2O$ (1.04 g, 2.0 mmol) and 3,5-Me_2pzH (197 mg, 2.0 mmol) were added to methanol (100 mL). The solution was heated at reflux under Ar (g) for 8 h and cooled to room temperature. The mixture was filtered and 2 mL of a saturated solution of NH_4PF_6 (aq.) was added to the red filtrate. The volume was reduced to 50 mL and then the solution was poured into 800 mL of diethyl ether. The resultant precipitate was collected by vacuum filtration. The red solid was washed with diethyl ether (3 × 20 mL) and dried under vacuum; yield 1.17 g (85%). $C_{25}H_{24}ClF_6N_6PRu$ (689.99): calcd. C 43.52, H 3.51, N 12.18; found C 43.58, H 3.55, N 11.98. ^1H NMR (CD_2Cl_2): δ = 1.19 (s, 3 H, CH_3), 2.23 (s, 3 H, CH_3), 5.77 (s, 1 H, CH_{Me2pzH}), 7.11 (m, 2 H, CH), 7.51 (d, 1 H, CH), 7.54 (dd, 1 H, CH), 7.65 (dd, 1 H, CH), 7.77 (m, 3 H, CH), 8.02 (m, 2 H, CH), 8.20 (m, 2 H, CH), 8.29 (d, 1 H, CH), 8.35 (d, 1 H, CH), 8.39 (d, 1 H, CH), 9.97 (d, 1 H, CH), 12.20 (s, 1 H, NH) ppm; see Figures S9–S10. ESI-MS (positive ion mode): *m*/*z* = 545.03 $[Ru(bpy)_2(Cl)(3,5\text{-}Me_2pzH)]^+$, 509.01 $[Ru(bpy)_2(3,5\text{-}Me_2pzH)]^+$, 448.88 $[Ru(bpy)_2(Cl)]^+$, 412.99 $[Ru(bpy)_2]^+$; see Figures S17–S18.

$[Ru(bpy)_2(Cl)(L)]^0$ (L = pz, 4-Mepz, and 3,5-Me_2pz): The ligand-deprotonated, pyrazolate complexes (**1**, **2**, and **3**) were generated in situ by addition of 1.2 equiv. of tetramethylammonium hydroxide (Me_4NOH; Aldrich) to the ligand-protonated, pyrazole species (**1H**, **2H**, and **3H**) in dry acetonitrile.

Acid-Base Experiments: Britton–Robinson (BR) buffer[17] (pH 2–12) was used to prepare aqueous (10% acetonitrile) solutions of the complexes in spectrophotometric titrations for pK_a determinations. The pH of the deoxygenated solutions was finely adjusted by the controlled microvolumetric additions of 3.0 M NaOH or trifluoroacetic acid (HTFA) solutions, as required.

Physical Measurements: ^1H NMR spectra were collected at 298 K using a Bruker DRX-500 instrument. Spectral signals from solvents (CD_2Cl_2 or CD_3CN) were used as internal resonances. Electrospray ionization (ESI) mass spectrometry was performed using an Applied Biosystems QStar XL instrument equipped with a Protana Nanospray source. Samples were introduced into a coated spray needle and mounted onto the nanospray source. Elemental analyses were carried out by Atlantic Microlab (Norcross, GA). UV/Vis absorption spectra were recorded on a Cary 300 spectrophotometer. A Bioanalytical Systems model CV-50W or Epsilon potentiostat was used in electrochemical experiments. In cyclic voltammetry (CV), a standard three-electrode setup consisted of a Pt disk working electrode, a Pt wire auxiliary electrode, and a saturated calomel electrode (SCE) as the reference electrode.[18] All sample solutions were purged with an Ar (g) stream. Infrared spectra of solution

samples were collected with a Perkin–Elmer Spectrum 400 FT-IR instrument (spectra were averages of 32 scans at a resolution of 1 cm^{-1}). Electrochemical and spectroscopic experiments were conducted at room temperature. The pH values of aqueous solutions were measured with a Thermo Orion 250A+ digital pH meter. Instrument calibration was performed using commercial standard buffers at pH 4.00, 7.00 and 10.00.

X-ray Crystallography: The crystal was mounted in a nylon cryoloop from Paratone-N oil under argon gas flow. The data were collected with a Bruker D8 diffractometer, with APEX II charge-coupled-device (CCD) detector, and an American Cryoindustries Cryocool G2 cryostat. The instrument was equipped with graphite-monochromatized Mo-K_α X-ray source (λ = 0.71073 Å), and MonoCap X-ray source optics. A hemisphere of data was collected using ω scans, with 10-second frame exposures and 0.3° frame widths. Data collection and initial indexing and cell refinement were handled using APEX II software.[19] Frame integration, including Lorentz-polarization corrections, and final cell parameter calculations were carried out using SAINT+ software.[20] The data were corrected for absorption using a multi-scan technique and the SADABS program.[21] Decay of reflection intensity was monitored via analysis of redundant frames. The structure was solved using Direct methods and difference Fourier techniques. All hydrogen atom positions were idealized, and rode on the atom they were attached to. The final refinement included anisotropic temperature factors on all non-hydrogen atoms. Structure solution, refinement, graphics, and creation of publication materials were performed using SHELXTL.[22] The crystal and refinement parameters are listed in Table 3.

Table 3. Summary of X-ray crystallographic data, intensity collection, and structure refinement parameters for **3H**·PF_6.

Empirical formula	$C_{25}H_{24}ClF_6N_6PRu$
Formula weight	689.99 g/mol
Temperature	120(1) K
Wavelength (Mo-K_α)	0.71073 Å
Crystal system	monoclinic
Space group	$P2_1/n$
Unit cell dimensions	a = 12.102(2) Å
	b = 16.826(3) Å
	c = 13.016(2) Å
	α = 90°
	β = 92.606(2)°
	γ = 90°
Volume	2647.6(8) $Å^3$
Z	4
Density (calculated)	1.731 mg/m^3
Absorption coefficient	0.824 $[mm]^{-1}$
$F(000)$	1384
Crystal size	$0.22 \times 0.16 \times 0.14$ mm^3
θ range for data collection	1.98 to 25.32°
Index ranges	$-14 \le h \le 14$,
	$-20 \le k \le 20$,
	$-15 \le l \le 15$
Reflections collected	25132
Independent reflections	4800 [R(int) = 0.0648]
completeness to θ = 25.00°	100.0%
Absorption correction	semi-empirical from equivalents
Max. and min. transmission	0.8933 and 0.8394
Refinement method	full-matrix least-squares on F^2
Data/restraints/parameters	4800/0/363
GOF on F^2	1.082
final R indices [$I > 2\sigma(I)$]	R_1 = 0.0343, wR_2 = 0.0783
R Indices (all data)	R_1 = 0.0489, wR_2 = 0.0856
Largest diff. peak and hole	0.692 and –0.465 e $Å^{-3}$

CCDC-707589 contains the supplementary crystallographic data for for **3H**·PF_6. These data can be obtained free of charge from The Cambridge Crystallographic Data Centre via www.ccdc.cam.ac.uk/data_request/cif.

Supporting Information (see also the footnote on the first page of this article): ^{1}H NMR spectra (Figures S1–S12) and ESI mass spectra (Figures S13–S18).

Acknowledgments

This work was supported by the U.S. Department of Energy through the Laboratory Directed Research & Development (LDRD) program at LANL. The technical assistance of Dr. R. Michalczyk (NMR) and Dr. S. Iyer (mass spectrometry) is gratefully acknowledged.

[1] a) A. Juris, V. Balzani, F. Barigelletti, P. Belser, A. von Zelewsky, *Coord. Chem. Rev.* **1988**, *84*, 85; b) V. Balzani, A. Juris, M. Venturi, S. Campagna, S. Serroni, *Chem. Rev.* **1996**, *96*, 759; c) E. C. Constable, *Chem. Soc. Rev.* **2007**, *36*, 246.

[2] a) S. Trofimenko, *Chem. Rev.* **1972**, *72*, 497; b) S. Trofimenko, *Prog. Inorg. Chem.* **1986**, *34*, 115; c) G. La Monica, G. A. Ardizzoia, *Prog. Inorg. Chem.* **1997**, *46*, 151; d) S. Trofimenko, *Scorpionates: The Coordination Chemistry of Poly(pyrazolyl) borate Ligands*, Imperial College Press, London, **1999**; e) R. Mukherjee, *Coord. Chem. Rev.* **2000**, *203*, 151; f) A. P. Sadimenko, *Adv. Heterocycl. Chem.* **2001**, *80*, 157, g) C. Pettinari, R. Pettinari, *Coord. Chem. Rev.* **2005**, *249*, 525; h) H. R. Bigmore, S. C. Lawrence, P. Mountford, C. S. Tredget, *Dalton Trans.* **2005**, 635.

[3] B. P. Sullivan, D. J. Salmon, T. J. Meyer, J. Peedin, *Inorg. Chem.* **1979**, *18*, 3369.

[4] a) S. Baitalik, U. Florke, K. Nag, *Inorg. Chem.* **1999**, *38*, 3296; b) S. Baitalik, U. Florke, K. Nag, *J. Chem. Soc., Dalton Trans.* **1999**, 719; c) S. Baitalik, U. Florke, K. Nag, *Inorg. Chim. Acta* **2002**, *337*, 439; d) V. J. Catalano, T. J. Craig, *Inorg. Chem.* **2003**, *42*, 321; e) C. Sens, I. Romero, M. Rodriguez, A. Llobet, T. Parella, J. Benet-Buchholz, *J. Am. Chem. Soc.* **2004**, *126*, 7798; f) H. Jude, F. N. Rein, P. S. White, D. M. Dattelbaum, R. C. Rocha, *Inorg. Chem.* **2008**, *47*, 7695.

[5] W. R. Browne, R. Hage, J. G. Vos, *Coord. Chem. Rev.* **2006**, *250*, 1653.

[6] a) A. Bond, M. Haga, *Inorg. Chem.* **1986**, *25*, 4507; b) M. Haga, T. Ano, K. Kano, S. Yamabe, *Inorg. Chem.* **1991**, *30*, 3843; c) C. G. Cameron, P. G. Pickup, *Chem. Commun.* **1997**, 303; d) P. Majumdar, S.-M. Peng, S. Goswami, *J. Chem. Soc., Dalton Trans.* **1998**, 1569; e) J. W. Slater, D. M. D′Alessandro, F. R. Keene, P. J. Steel, *Dalton Trans.* **2006**, 1954; f) M. Murali, M. Palaniandavar, *Dalton Trans.* **2006**, 730.

[7] R. C. Rocha, H. E. Toma, *J. Coord. Chem.* **2004**, *57*, 303.

[8] a) F. Barigelletti, L. De Cola, V. Balzani, R. Hage, J. G. Haasnoot, J. Reedijk, J. G. Vos, *Inorg. Chem.* **1989**, *28*, 4344; b) R. Hage, J. G. Haasnoot, H. A. Nieuwenhuis, J. Reedijk, D. J. A. De Ridder, J. G. Vos, *J. Am. Chem. Soc.* **1990**, *112*, 9245; c) J. G. Haasnoot, *Coord. Chem. Rev.* **2000**, *200–202*, 131; d) R. C. Rocha, H. E. Toma, *Polyhedron* **2003**, *22*, 1303; e) R. C. Rocha, H. E. Toma, *Transition Met. Chem.* **2003**, *28*, 43; f) D. M. D'Alessandro, P. H. Dinolfo, J. T. Hupp, P. C. Junk, F. R. Keene, *Eur. J. Inorg. Chem.* **2006**, 772; g) C. Richardson, C. M. Fitchett, F. R. Keene, P. J. Steel, *Dalton Trans.* **2008**, 2534.

[9] D. S. Eggleston, K. A. Goldsby, D. J. Hodgson, T. J. Meyer, *Inorg. Chem.* **1985**, *24*, 4573.

[10] Infrared spectroscopy was used to make a direct comparison between the ν(N–H) frequency for the free ligand Me_2pzH (3370 cm^{-1}; strong, broad) with that of the coordinated ligand in **3H** (3230 cm^{-1}; weak-to-medium, broad) in acetonitrile. The large frequency downshift of 140 cm^{-1} is in agreement with a strong N–H···Cl interaction.

[11] a) D. Carmona, J. Ferrer, L. A. Oro, M. C. Apreda, C. Focesfoces, F. H. Cano, J. Elguero, M. L. Jimeno, *J. Chem. Soc., Dalton Trans.* **1990**, 1463; b) M. M. T. Khan, P. S. Roy, K. Venkatasubramanian, N. H. Khan, *Inorg. Chim. Acta* **1990**, *176*, 49.
[12] M. Onishi, M. Yamaguchi, S. Kumagae, H. Kawano, Y. Arikawa, *Inorg. Chim. Acta* **2006**, *359*, 990.
[13] R. M. Hartshorn, R. Zibaseresht, *Arkivoc* **2006**, 104.
[14] B. P. Sullivan, D. Conrad, T. J. Meyer, *Inorg. Chem.* **1985**, *24*, 3640.
[15] a) G. Yagil, *Tetrahedron* **1967**, *23*, 2855; b) ACD/Labs pK_a Database, version 10.0, Advanced Chemistry Development, Inc., Toronto, ON, Canada, **2007**.
[16] B. P. Sullivan, D. J. Salmon, T. J. Meyer, *Inorg. Chem.* **1978**, *17*, 3334.
[17] H. T. S. Britton, R. A. Robinson, *J. Chem. Soc.* **1931**, *458*, 1456.
[18] This SCE reference electrode gave a half-wave potential ($E_{1/2}$) of 0.41 V for the ferrocene/ferrocenium couple.
[19] *APEX II 1.08*, Bruker AXS, Inc., Madison, WI 53719, **2004**.
[20] *SAINT+ 7.06*, Bruker AXS, Inc., Madison, WI 53719, **2003**.
[21] G. Sheldrick, *SADABS 2.03*, University of Göttingen, Germany, **2001**.
[22] *SHELXTL 5.10*, Bruker AXS, Inc., Madison, WI 53719, **1997**.
Received: November 5, 2008
Published Online: January 14, 2009

